LAWRENCE
LIVERMORE
NATIONAL
LABORATORY

LLNL-CONF-413290

# Axial-Torsion Testing Plastic-Bonded Explosives to Failure

F. J. Gagliardi, B. J. Cunningham

May 26, 2009

2009 SEM Annual Conference
Albuquerque, NM, United States
June 1, 2009 through June 4, 2009

## Disclaimer

# Axial-Torsion Testing Plastic-Bonded Explosives to Failure

Franco J. Gagliardi, gagliardi7@llnl.gov
Bruce J. Cunningham, cunningham1@llnl.gov

Lawrence Livermore National Laboratory
Energetic Materials Center
P.O. Box 808, L-282, Livermore, CA 94550, USA

ABSTRACT: Performing multi-mode loading of plastic-bonded explosives (PBXs) to failure is necessary to developing realistic constitutive material models. Axial-torsion testing of LX-14 was performed to develop an understanding of the failure mechanisms associated with composite explosive materials under combined loading conditions. The material tested was a bi-phase composite PBX that was 95.5% HMX, a crystalline explosive material, mixed with 4.5% Estane, a polymeric binder. The tests were run at a constant angular velocity, over a range of compressive loads (held constant during each test), with compressive stresses ranging from 0 to 19.9 MPa, and at room temperature. Tests were performed using an MTS servo-hydraulic unit equipped with custom designed supporting tubes. The geometry of the part and the maximum torque value were used to compute the maximum shear stress. Test results showed that the mode of failure was either shear or tensile, depending on the applied compressive stress magnitude. The experimental technique, test results, and analyses are presented as well as a discussion of the use of digital image correlation to observe the strain development leading to failure.

## INTRODUCTION

Plastic-bonded explosives (PBXs) are composite materials that are typically a mixture of two components: explosive crystals and a polymeric binder. The ratio of the explosive component to the binder varies from one material to the next, but, typically, the explosive portion comprises 80-95% of the mass of the composite [1]. One benefit of the presence of binder is the reduction in the composite's sensitivity. This occurs because the binder coats the explosive crystals and acts as a barrier between them, reducing heat generation created by friction during deformation [2]. Another benefit is that PBX composites have superior mechanical strength compared to pure explosive parts, allowing precision parts to be machined from the compacted material [3]. Precision geometries are important features in systems where detonation propagation needs to be highly predictable.

Many types of testing are used to characterize the mechanical properties of various PBXs, including quasi-static uni-axial compressive, and uni-axial tensile tests. Uni-axial tension and compression tests are used as a means of characterization for nuclear stockpile certification, material model development, and new lot qualification [4]. These tests provide the much-needed information for the development and validation of accurate material models. In the 2007 we reported on the development of a creep system to provide data to help in this validation [5]. The development of such models allows us to examine the material response of various charge configurations to diverse load and thermal conditions.

In real-world PBX applications, multi-axial stress conditions are present and need to be understood. To assist in the effort to understand the complex nature of multi-axial loading and failure, we are working to develop tests that will provide an accurate means of measuring the material response to complex load conditions.

Past work has included the study of PBX material properties under various forms of uni-axial load. As time has passed and additional information has been obtained about the uni-axial behavior of these materials, we have

begun to examine more complex stress conditions. To achieve this goal, LX-14 samples were tested under combined loading conditions. LX-14 is a bi-phase composite PBX that consists of 95.5% HMX, a crystalline explosive material, mixed with 4.5% Estane, a polymeric binder [6]. The results from this effort helped us to develop a greater understanding of the failure mechanisms associated with composite explosive materials under combined loading conditions, and the test series is the focus of this paper.

## MULTIL-AXIAL TESTING

Recent work done at LLNL has focused on the development of a multi-axial testing capability and results from this type of testing have been used to further enhance our understanding of the behavior of PBX materials under combined loading. Prior to the acquisition of an MTS Axial-Torsion Load Unit in 2006, we did not have the tools needed to perform tests in which samples could be simultaneously axially and torsionally loaded. The hardware acquired to perform these tests included an MTS Series 858 hydraulically controlled system equipped with an axial load capacity of 5.5 Kips (24.5 kN) and a torque capacity of 2000-in-lbs (226 N-m). The system is capable of running in axial displacement, angular displacement, axial load and/or torque control. At the time that the tests reported in this paper were conducted, the system we had did not have the means to measure shear strain. Since that time, we have acquired a Digital Image Correlation (DIC) system, and that system will be used in the future to measure the shear strain field on the surface of our samples.

## MATERIAL

The specimens used in our axial-torsion tests were machined from a pressed billet of LX-14 molding powder. The molding powder was manufactured by Holston and had the lot designation HDC96E266-003, Blend 510. The billet was subsequently machined into 1-inch by 1-inch by 0.875-inch square cuboids. The cuboids were then further machined into the final geometry shown in Fig. 1. The final specimen had a central tube-shaped region that had an outer diameter of 0.825-inch and an inner diameter of 0.625-inch. The square ends of the specimen were approximately 0.135-inch thick.

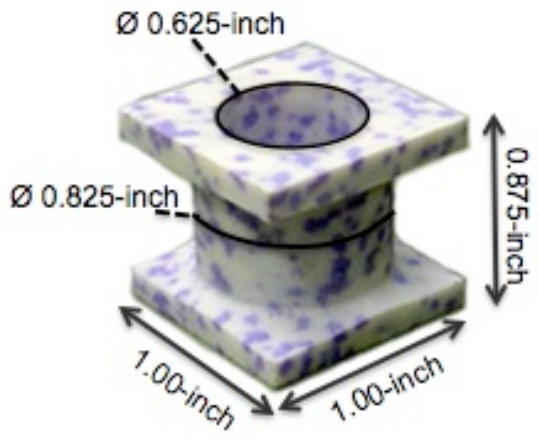


**FIGURE 1: An LX-14 axial-torsion specimen, machined from a billet. The dimensions of this specimen are 1-inch by 1-inch by 0.875-inch, with an outer diameter of 0.825-inch and an inner diameter of 0.625-inch. The set of specimens used in this study were pressed and machined in the late 1990s.**

The samples had been pressed and machined in the late 1990s but had remained in storage until recently because of a lack of equipment necessary to perform the type of tests for which they were intended

## EXPERIMENTAL PROCEDURE

The test variables for axial-torsion testing included axial load, axial load application (i.e., timing), angular-displacement rate and test temperature.

The geometry of the samples used in this study required the design and fabrication of rigid aluminum adapter rods that were capable of transmitting the torque from the load unit through the sample and into the torque cell. Attached to the sample ends of the aluminum adaptor rods were bracket grips that were used to center the specimen and hold it in place during the test. Each grip plate had three adjustable aluminum brackets that were used in concert to support the sides of the sample. A precisely positioned sample-centering pin was attached to the center of the top grip plate. Fig. 2 is a picture of the central portion of the axial-torsion fixture, highlighting the aluminum torsion rods, the aluminum mount plates and the centering pin. The aluminum torsion rods acted as rigid adaptors, coupling the system to the sample. The centering pin had an outer diameter slightly less than the inner diameter of the PBX specimen (i.e., 0.625-inch) and was designed so that it could be easily taken out prior to testing, once the sample was secured in the upper grips. Fig. 3 shows an LX-14 specimen in the axial-torsion fixture prior to the removal of the centering pin. After removal of the centering pin,

the upper portion of the fixture and the sample were slowly lowered into position and then the grips of the lower plate were adjusted and tightened so that both the top and the bottom of the sample were secured.

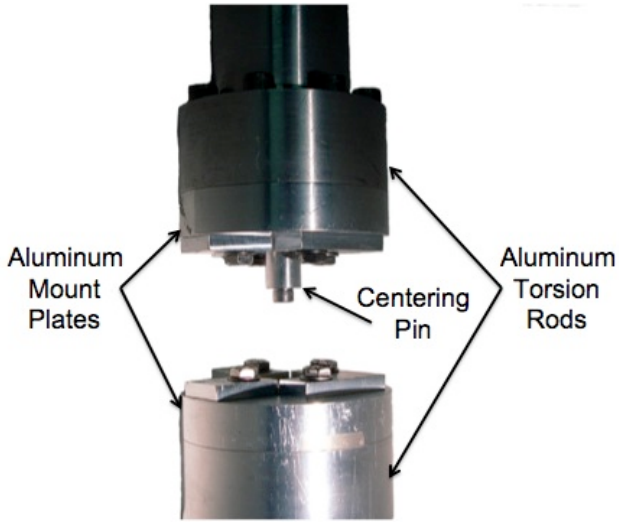


**FIGURE 2: Axial-torsion fixture showing the upper and lower aluminum torsion rods, the upper and lower aluminum mounts plates and the sample-centering pin.**

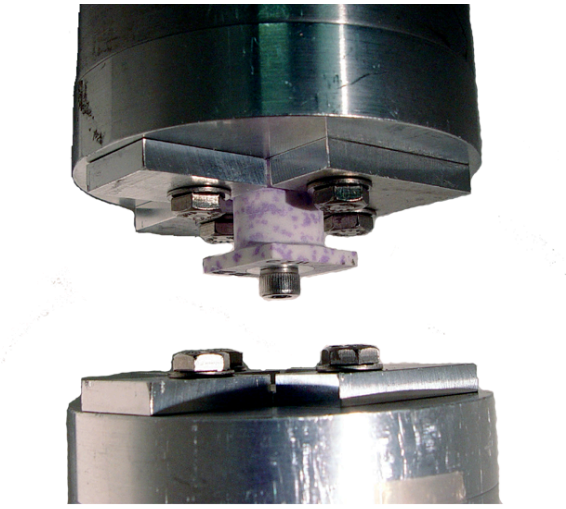

**FIGURE 3: Axial-torsion fixture with LX-14 sample in place. After the upper brackets are tightened, the centering pin is removed and the upper rod, with the sample attached, is lowered into place. Then the lower brackets are tightened and testing can commence.**

The test series consisted of running multiple tests in torsion, (with the exception of the uniaxial tension and compression tests) and at varying levels of compressive load. Tests were performed at a constant rate of angular-displacement and at room temperature (~25˚C). The angular velocity of the upper grip relative to the lower grip was programmed to 0.08-deg/s for all of the tests that included rotation. This angular-displacement rate was chosen because it produced a shear strain rate of approximately 0.001-in/in/s through the centerline of the tube's cross-section. This rate was desirable because it was similar to axial strain rates typically used at LLNL. Rate control is especially important when measuring the mechanical properties of PBX materials because they are highly strain rate dependent.

The torque level was monitored and recorded throughout each test. Following each test, the peak torque value was determined so that a sample-to-sample comparison could be made of peak torque as a function of the applied axial load. Post test, the fractured specimens were examined for evidence of the mode in which they experienced failure.

## RESULTS

In this section, the results of nine tests (7 multi-axial and 2 uni-axial) are presented. A pure tensile test and a pure compressive test were run to characterize the uni-axial material behavior of LX-14. Seven samples were tested using different amounts of compressive load, in conjunction with a constant angular velocity of 0.08-deg/s. For the nine tests, the axial force in Newtons, the axial stress in MPa, the maximum torque in N-m and the average maximum applied shear stress (based on the maximum torque) in MPa are reported in Table 1.

For reasons of convenience, the test run in pure tension used a sample that had our standard "dog-bone" geometry (3-in long, with a 0.5-in diameter constant diameter cross-section) Samples with this geometry are often used in uni-axial tensile testing of PBX materials at LLNL. This particular tensile specimen had been made from the same lot of material and at the same time as the axial-torsion specimens described above. The remaining

eight tests used the axial-torsion specimen geometry shown above. The average applied in-plane shear stress was calculated from the maximum torque applied to the cross-section of the tube, the area of the annulus (1.47 x $10^{-4}$ $m^2$) and the average radius of the tube (9.2 x $10^{-3}$ m) in the relationship shown in Eq. 1:

$$\tau_{Ave.in-plane} = \frac{Torque}{Area_{Annulus} * Radius_{Ave.}} \quad (1)$$

**TABLE 1: Axial load conditions and torque and stress at failure data for the LX-14 axial-torsion test matrix.**

| | | | | | | | | | |
|---|---|---|---|---|---|---|---|---|---|
| **Axial Force (N)** | 587.2 | 0 | -22.2 | -444.8 | -1112 | -1646 | -1957 | -2331 | -2518 |
| **Axial Stress (MPa)** | 4.63 | 0 | -0.15 | -3.03 | -7.59 | -11.24 | -13.37 | -15.92 | -19.86 |
| **Torque (N-m)** | 0 | 6.21 | 6.82 | 7.6 | 9.4 | 9.89 | 8.59 | 9.04 | 0 |
| **Average Shear Stress (MPa)** | 0 | 4.59 | 5.05 | 5.62 | 6.95 | 7.31 | 6.35 | 6.68 | 0 |

Fig. 4 shows the torque versus angle data for the series of seven tests in which both axial stress and torque were applied to the specimens. The axial stress for each test represented in Fig. 4 is shown in the color of the torque vs. angle trace. The indicated angular rotation was not considered sufficiently reliable for use in shear strain calculations because of the resolution limitation of the angular displacement transducer, uncertainties having to do with the test system's torsional rigidity and suspected slippage at the grip/sample interface. Fig. 5 plots the maximum torque measured as a function of the applied axial stress for each specimen that underwent torsion.

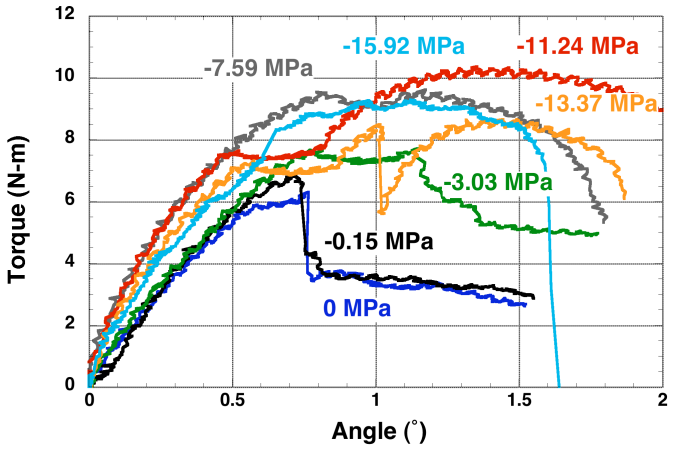


**FIGURE 4: Representative data showing torque as a function of angular rotation for the seven axial-torsion tests. The compressive stress applied to the samples ranged between 0 and 15.92-MPa. For each test, the fixed applied compressive stress is shown on the plot in the color that matches its corresponding torque vs. angle trace.**

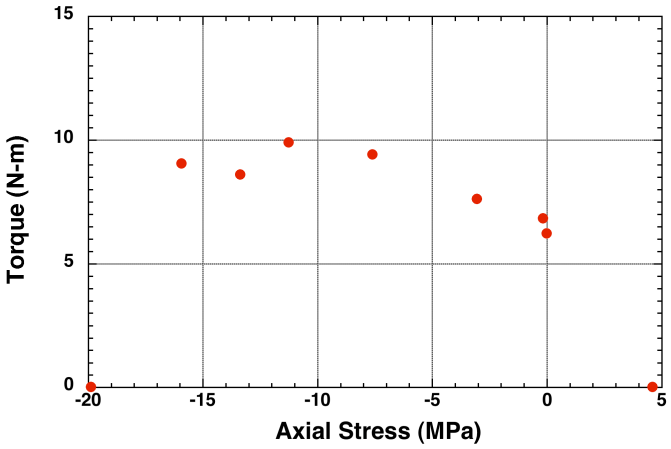


**FIGURE 5: Maximum torque data plotted as a function of the applied axial stress for the LX-14 specimens. The data points shown at zero torque were the failure stresses from tests run in pure tension (4.63 MPa) and pure compression (-19.86 MPa).**

ANALYSIS AND DISCUSSION

The post-test examinations revealed that under conditions of pure tension, pure torsion and at low levels of compression, the failure mode was tensile. This phenomenon was manifested by through-wall fractures that appeared around the tube in a “cork-screw” pattern at an angle of about 45˚. Fig. 6 shows a sample that failed in the tensile mode. Typically, PBX materials are weakest in tension and therefore will fail in tension unless combined loading conditions are present such that the internal tensile stresses are suppressed to the point that another stress threshold is reached first. With this in mind, as the applied axial stress level increased (i.e., the sample was subjected to greater compressive stresses), the failure mode changed from tensile to shear. Shear failure is manifested by a conical failure surface, like that shown in Fig. 7. The sample pictured in Fig. 7 was tested at -13.37 MPa axial stress, and in that case the axial stress was sufficiently great that shear failure occurred before the tensile threshold was reached.

The transition from the tensile mode of failure to the shear mode of failure in these combined loading tests was due to the fact that, as the axial stress increased, the tensile stresses in the sample were effectively suppressed, until the material began to fail in shear. In our standard compression tests at LLNL, solid cylinders of PBX material routinely fail in shear, a fact demonstrated by visible fracture lines that routinely appear at about 45˚ to the direction of the load.

**FIGURE 6: Fractured LX-14 Axial-torsion specimen showing characteristic failure of a specimen in tension. A diagonal crack is visible from the bottom left to top right of the sample. Failures such as these occur at low levels of applied compressive stress.**

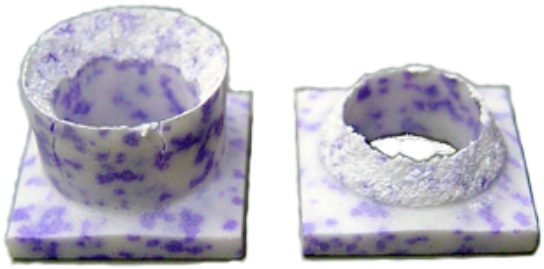

**FIGURE 7: Fractured LX-14 axial-torsion specimen showing characteristic failure of a specimen that has failed in shear. A diagonal fracture surface is visible from the outside to the inside of the tube wall. The fracture surface appears to start at the interface of the tube and the end section, a point of stress concentration.**

The use of the principal stress equations to compute various maximum stress values was helpful in understanding why the maximum torque curve looked as it did. The equations for the maximum shear stress and the principal stress values used for analysis are shown below [7]:

$$\tau_{Max} = \sqrt{\frac{\sigma_{Axial}^2}{4} + \tau_{Applied}{}^2} \qquad (2)$$

$$\sigma_{Max.Compression} = \sigma_{Min.} = \frac{\sigma_{Axial}}{2} - \tau_{Max.} \qquad (3)$$

$$\sigma_{Max.Tensile} = \sigma_{Max.} = \frac{\sigma_{Axial}}{2} + \tau_{Max.} \quad (4)$$

$$\sigma_{vonMises} = \sqrt{\sigma_{Axial}^2 + 3 \cdot \tau_{\text{Applied}}{}^2} \quad (5)$$

Eq. 2-5 are plotted in Fig. 8 along with the average applied shear stress as determined using the maximum torque values from the experiments and Eq. 1. The dashed horizontal lines indicate the upper limit of the maximum shear stress threshold and the upper limit of the maximum tensile stress threshold.

Eq. 2 and Eq. 4 were used to develop a maximum tensile stress threshold criteria and the equation was solved for the maximum torque:

$$Torque_{Max} = A \cdot r \cdot \sqrt{\left(\frac{\sigma_{Max.Tensile} - \sigma_{Axial}}{2}\right)^2 - \frac{\sigma_{Axial}^2}{4}} \quad (6)$$

Eq. 2 was solved for the maximum torque value and will henceforth be referred to as the shear stress failure threshold:

$$Torque_{Max} = A \cdot r \cdot \sqrt{\frac{\tau_{Max}^2 - \sigma_{Axial}{}^2}{4}} \quad (7)$$

Eq. 6 and 7 are plotted in Fig. 9 with the maximum experimental torque values versus the applied axial stress. These plots were dependent on the assumption that the maximum sustainable pure tensile stress was 4.63 MPa and the maximum shear stress (the shear failure stress) was 9.93 MPa (half of the maximum pure compressive stress). As shown in Fig. 9, the data fits well with the envelope created by the two threshold equations.

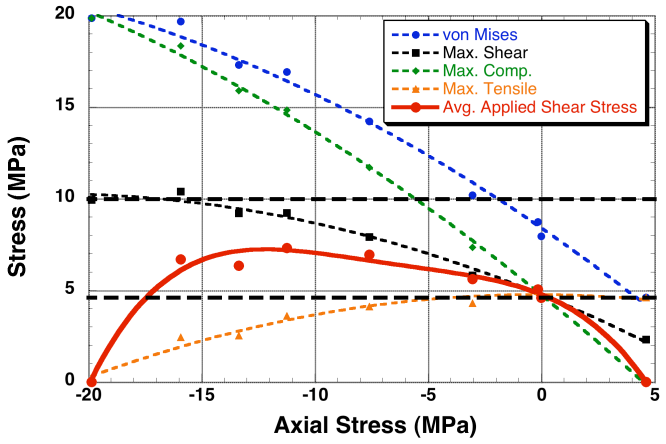


**FIGURE 8: Stresses calculated from the principle stress equations versus applied axial stress. Included are the theorized von Mises, maximum shear, maximum tensile and maximum compression thresholds calculated from Eq. 2-5. The horizontal dashed lines demarcate the upper limits seen by the maximum shear (higher level) and maximum tensile (lower level) thresholds. The experimental data seems to be well bounded by these two thresholds.**

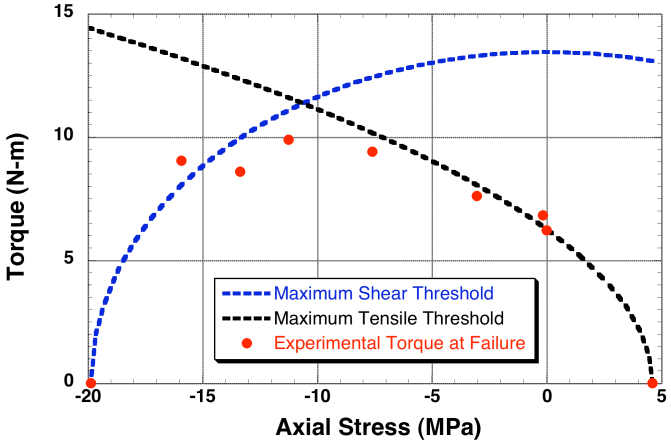


**FIGURE 9: Experimental torque versus applied axial stress data plotted with the theorized maximum shear and maximum tensile thresholds calculated from Eq. 6 and Eq. 7. The maximum shear stress used in Eq. 7 was -9.93 MPa, which is half of the maximum pure compressive stress measured at failure.**

It should be noted that there are several potential sources of error in these experiments. One possible source of error is non-uniformity of loading due to imperfections in the symmetry of the sample, or in the fixture. Another possible source of errors are stress concentrations in the sample, such as are present at the intersection between the square region of the sample and the tube section. A third possible source of error is the strain rate dependence of the material. When these tests were run, we had no capability in place for monitoring shear strain of the sample. In future testing, we hope to employ the use of a DIC system, and through doing so, we should be able to develop a better understanding of the three possible sources of error and their effect on experimental results.

## SUMMARY

This experimental series used specimens machined from LX-14 to examine the failure behavior of the PBX material in torsion under varying levels of compressive load. This material was selected because of its availability and its general similarities to other materials in which we have interest, primarily insensitive PBXs. The results from these experiments showed that the failure mode of the material was dependent on the level of applied axial stress. Samples failed in tension, as evidenced by their "cork-screw" fracture patterns, if the combined stresses were such that the maximum tensile stress threshold was reached. Whether this was the case was dependant on the amount of compressive stress, the geometry of the sample and the uni-axial tensile strength of the material. As the applied compressive stress was increased, a limit was reached where the specimen's failure mode transitioned to shear. This occurred because the applied compressive stress acted, increasingly, to suppress the tensile stress in the sample. At the transition, the sample began to reach the shear failure threshold prior to reaching the tensile threshold, and so began failing in shear. Shear failure was evidenced by a 360-degree conical fracture extending through the tube wall.

In the future, we expect testing will focus on insensitive PBX materials and will begin utilizing the non-contact full-field strain measuring capability provided by DIC.

## AKNOWLEDGEMENTS

This work was performed under the auspices of the U.S. Department of Energy by Lawrence Livermore National Laboratory under Contract DE-AC52-07NA27344.

## REFERENCES

[1] Cooper, P. W. and Kurowski, S. R., *Introduction to the Technology of Explosives*, New York: Wiley-VCH, p. 21-23, 1996.
[2] Trevino, S. F. and Wiegand, D. A., "Mechanically Induced Damage in Composite Plastic-Bonded Explosives: A Small Angle Neutron and X-ray Study," *Journal of Energetic Materials,* 26: 79-80, 2008.
[3] Cooper P. W. and Kurowski, S. R., *Introduction to the Technology of Explosives*, New York: Wiley-VCH, p. 21, 1996.
[4] Thompson, D. G. and Wright, W. J., "Mechanical Properties from PBX 9501 Pressing Study," *Meeting of the Topical Group on Shock Compression of Condensed Matter of the APS* (20-25 Jul 2003), Portland, OR, AIP Conf. Proc., 706, no. 1, p. 503, 2004.
[5] Gagliardi, F. J. and Cunningham, B. J., "Creep Testing Plastic-Bonded Explosives in Uni-axial Compression," SEM XI International Congress & Exposition Proceedings, June 2008.
[6] DoBratz, B. M. (Ed.), *Lawrence Livermore National Laboratory Explosives Handbook*, UCRL-52997, Revised January 1985.
[7] Seely, M. S. and Smith, J. O., *Advanced Mechanics of Materials*, New York: Wiley & Sons, Inc., p. 56-57, 1967.